A Summary Report on Assembly 3 of FRO

T. L. Andersson, B. Brunfelter, P. F. Cecchi, E. Hellstrand, J. Kockum, S-O. Londen and L. I. Tirén



AKTIEBOLAGET ATOMENERGI STOCKHOLM, SWEDEN 1966

A SUMMARY REPORT ON ASSEMBLY 3 OF FRO

T. L. Andersson, B. Brunfelter, P. F. Cecchi, E. Hellstrand, J. Kockum, S-O. Londen and L. I. Tirén

ABSTRACT

The third core of the zero energy fast reactor FR0 consisted of 20 % enriched uranium diluted to 29 vol. % with graphite and had a volume of 50 litres. Like previous cores it was surrounded by a thick copper reflector. The report summarizes measurements of critical mass, control rod reactivities, fine structure flux variations and conversion ratio. In particular, effects associated with the heterogeneous arrangement of the uranium and graphite plates are examined.

LIST OF CONTENTS

	LIST OF CONTENTS	Page
1.	Introduction	3
2.	Critical mass determination	4
2.1	Core loading and approach to criticality	4
2.2	Corrections to loaded mass	5
3.	Control rod calibrations	6
4.	Flux variations due to the heterogeneous loading	7
4.1	Purpose of experiment	7
4.2	Modification in loading pattern	7
4.3	Foil irradiations	7
4.4	Activity measurements	8
4.5	Results	9
5.	Conversion ratio measurements	12
5.1	Introduction	12
5.2	Experimental details	12
5.3	Results and comparison with theory	13
Ackn	owledgements	16
Refe	rences	17

Figures

1. INTRODUCTION

This report presents experimental results obtained on Assembly 3 of FRO. Much of the work has already been reported in internal memos, but it has been considered worth while to summarize some of the effort in one document. However, the central reactivity experiments as well as the measurements of fission and capture rates and fission ratios have been described in great detail in published reports [1, 2], and therefore no account of those experiments is given here. The analysis of the pulsed source measurements of reactivity and prompt neutron life-time is still at a preliminary stage, pending further calculations with the time dependent $S_{\rm M}$ code, and will be reported separately.

The composition of Assembly 3 is given in Table 1. The graphite dilution was effectuated in order to provide a fairly soft neutron spectrum. As a matter of fact the degree of softening obtained was rather low, but a further dilution with graphite was not practicable since the critical mass would then exceed the limit set by our inventory of U235 (120 kg). The calculated value of the median fissioning energy (for U235) in Assembly 3 was 270 keV as compared with 360 keV in the undiluted Assemblies 1 and 2.

A description of the FRO reactor is given in [3].

Table 1. Core composition

Material	Volume	%	Atomic density atoms/cm ³ x 10 ⁻²²
Uranium	58.5		
U235	,	11.7	0.568
U238		46.8	2.234
Steel	6.5	,	
Fe		4.8	0.408
Cr		1.2	0.0962
Ni		0.5	0.0475
Graphite	29.2		2.47
Teflon (CF ₂)	0.1		0.003

T (1			• . •
Retie	CLOT	compo	gition
	~~~	0044100	0202011

Material	Volume %	Atomic density atoms/cm ³ x 10 ⁻²²
Copper	88.5	7.48
Steel	6.5	
Fe	4.8	0.408
Cr	1.2	0.0962
Ni	0.5	0.0475

#### 2. CRITICAL MASS DETERMINATION

## 2.1 Core loading and approach to criticality

The core was built as an approximate cylinder with a height of 38.7 cm and equivalent diameter of 40.8 cm. The loading pattern is shown in Fig. 1. The 3.55 mm thick graphite plates were staggered as shown in Fig. 2a in order to achieve as homogeneous a pattern as possible. The core was surrounded by a copper reflector sufficiently thick (about 35 cm) to be regarded as infinite.

Critical mass calculations were performed using the DSN (14 groups) and TDC (6 groups) codes and a cross section set compiled by Häggblom. The cross section set was identical with "set 2" [5], except for the U235(n,f) and Cu(n, $\gamma$ ) cross section data in which new experimental information was taken into account. The modified cross section set was called set 2B and the modifications are specified in [2]. The values obtained were:

DSN code (	(sphere)	1	10	kg	U235*
TDC code	(cylinder	) 1	11.9	kg	<b>U</b> 235

A stepwise approach to criticality was used, the first two steps being 50 and 75 % of the calculated mass. The subsequent steps were determined in the usual way using plots of the inverse pulse rates from suitably positioned BF₃ chambers as a function of the loaded mass. Criticality was reached in the seventh step, the loaded mass then being 111.4 kg U235.

^{*}Including a shape factor of 0.96 [3].

## 2.2 Corrections to loaded mass

In order to obtain a critical mass value for the equivalent homogeneous cylindrical core corrections for the following effects were made:

- a) Core edge irregularity
- b) Excess reactivity of the fine control rod
- c) Reactivity effect of the source access channel
- d) Core heterogeneity.

The core edge irregularity correction was determined by measuring the difference in reactivity between the uranium-graphite "mixture" and copper at different radial positions close to the core-reflector boundary. The result is illustrated in Fig. 3. This curve was used in conjuction with the ALIT-1 programme [3] to give the desired correction factor.

The corrections a), b) and c) together produced a reduction in mass of 1.4 kg U235.

The effect of heterogeneity was estimated by measuring the reactivity change produced when rearranging the plates in an ordinary fuel element in such a way as either to increase or reduce the plate thicknesses (see Fig. 4). The measurement was made by the positive period technique. The reproducibility was limited to about  $\pm 1 \times 10^{-5}$  by the necessity to shut down the reactor between the reloadings.

In Fig. 4 the normal plate arrangement in a fuel element is denoted 4P. The corresponding plate dimensions are 4.3 x 4.3 x 0.71 cm for the uranium plates (20 % U235) and 4.3 x 4.3 x 0.355 cm for the graphite plates. The element was placed at various distances from the core centre and the reactivity change corresponding to the 4P to 1P rearrangement was measured. In the case of the other rearrangements (2P and 8P) the whole row of fuel elements in positions Fall - Fal9 (see Fig. 1) were reloaded simultaneously and the spatial dependence found in the 4P to 1P rearrangement was assumed to prevail. This spatial dependence is shown in Fig. 5. It is interesting to note that the reactivity change is largest at some distance from the core centre. This indicates that leakage as well as absorption effects contribute to the net reactivity change.

The heterogeneity correction was obtained by extrapolating the curve to zero plate thickness. A decrease in reactivity of (0.195  $\pm$  0.020) x 10⁻² is obtained.

According to Fig. 3 the reactivity worth of uranium at the core reflector boundary is  $34 \cdot 10^{-5}/\text{kg U}$ ; hence the homogeneous core would have a critical mass of U235 (1.14 ± 0.14) kg larger than the loaded heterogeneous core, a correction of 1%.

Applying the various corrections a critical mass value of the homogeneous cylindrical core of 111.1 kg U235 is obtained. This figure is in good agreement with the value obtained from the calculations.

## 3. CONTROL ROD CALIBRATIONS

The reactivity of the control rods was measured by the following methods:

Safety rods (SCS): Rod drop

Start rods (STS): Inverse multiplication

Fine control rod (FKS): Positive period.

The positions of the various rods are shown in Fig. 7. The methods and applications to FRO have been described in detail in [4], where theoretical comparisons have also been reported. In this report, therefore, only the experimental results are given. These are shown in Table 2 and in Figs. 8 and 9.

Table 2. Total worths of control rods

Rod No.	Position	Reactivity %
FKS	Fd12	0.229
STSI	Rb16	1.05
STS3	Fb12	0.78
SCS1	Rb12	0.75
SCS4	Fb14	1.17
SCS6	Fd14	0.81

# 4. FLUX VARIATIONS DUE TO THE HETEROGENEOUS LOADING

## 4.1 Purpose of experiment

The heterogeneity of the core loading discussed in Section 2 also causes variations in the neutron flux within the plates. Information about these flux variations was obtained by irradiating thin foils placed at various positions in the uranium-graphite pattern and measuring the activity on the foils after irradiation. Several foil materials were used having different neutron energy response. In this way some information concerning the spectrum dependence of the fine structure variations was also obtained.

## 4.2 Modification in loading pattern

The normal loading pattern of a fuel element is staggered as shown in Fig. 2a and a section of the core loading has the pattern shown in Fig. 1. This arrangement was chosen rather than a slab-like configuration (Figs. 2b and 10) which represents a more heterogeneous geometry. In connection with the fine structure experiment, on the other hand, a simple slab geometry is advantageous, since in this case comparison with theoretical results is more easy. Consequently a slab arrangement as shown in Figs. 2b and 10 was made up in the central core region where the flux measurements were made. Simultaneously the layers of fuel and graphite plates were made twice as thick as in the normal arrangement. The reason for the latter change was twofold:

- 1. The thickness of the foils used for the flux measurements involves a relatively less distortion when the layers are thick.
- 2. The magnitude of the flux variations is larger the thicker the layers of plates, and hence the relative errors become smaller.

## 4.3 Foil irradiations

Foil materials with different energy response were used in the fine structure measurements. The properties of the different foils are listed in Table 3. Their shapes were either circular with a diameter of 12 or 17 mm, or square with a side length of 10 mm.

Table 3.

Element	Reaction	Approximate neutron cut-off energy[1]	Measured activity	Half life	Foil thickness mm
Inl15	n,n'γ	1.5 MeV	E(γ)=335 keV	4.5 h	1.0
U238*	n,f	1.4 MeV	E <b>(</b> γ)>660 keV	-	0.3
Cu63	n,γ	-	β	12.8 h	0.2
U238**	n,γ	-	E(γ)≈100 keV	2.3 d	0.05
Mn55	n,γ	-	β	2.6 h	0.2

^{*} Depleted: 0.04 % U235.

During the irradiation the foils were wrapped in thin aluminium foils in order to prevent fission product contamination. All foils were irradiated in adjacent fuel elements, close to the core axis, where the radial flux gradient is small. Either the elements Fal5 and Ral5 or Fal6 and Ral6 were used (see Fig. 10).

Two different locations in the core region of these elements were chosen, (see Fig. 2b). The first location (No. 1) was at the centre of the elements in the equilibrium core spectrum, and the second location (No. 2) was at the core-reflector interface where the neutron spectrum is softer. In the latter case the U238(n,f) reaction was not employed.

Fig. 11a illustrates the loading of foils in two adjacent elements.

16 foils were inserted. The finite thickness of the foils made it necessary to remove one normal fuel plate in each element and to replace it by a thinner one and an aluminium filler plate. In the case of the thicker foils, In115 and U238(n,f), the number of foils loaded was only 8 (Fig. 11b). Small cavities were milled out of the graphite plates to allocate the thick foils but no corresponding device was possible at the fuel plates.

The foils were irradiated for 2 hours at a power level of 10 Watts corresponding to a dose of about  $5 \cdot 10^{12} \text{ n/cm}^2$ .

## 4.4 Activity measurements

The measurements on the irradiated foils were only relative in nature. For Mn and Cu integral  $\beta\text{--}counting}$  was employed using a  $\beta\text{--}$ 

^{**} Natural uranium.

scintillation crystal and photomultiplier set up. For the other foils the  $\gamma$ -activity was detected by means of NaI scintillation crystals. The Inl15 activity was measured over the 335 keV deexcitation  $\gamma$ -line using a multi-channel analyzer. The U238 capture rate was determined using the  $\gamma$ -X-coincidence apparatus described in [5]. Finally, the fission product activity of the U238 foils was measured by counting gamma rays above 660 keV, in which case no activity due to the  $(n,\gamma)$  reaction is present.

In addition to the detectors listed in Table 2, thin foils of a U235-Al alloy (5 mg U235/cm²) were also employed. The fission product  $\gamma$ -activity in the foils was measured in a manner similar to that used for the U238(n,f) reaction. In the case of the U235 foils, however, the net accuracy was only about 2 % due to the combined errors of counting statistics, weight intercalibration and uncertainties due to the non-exponential decay. This accuracy is insufficient in the present application, but the accuracy may be improved in future measurements. The measurements showed, however, that the amplitude of the U235(n,f) fine structure is not substantially larger than 2 % (peak-to-peak).

## 4.5 Results

The flux distributions measured with the different foils are shown in Figs. 12 and 13. The threshold reactions In115(n,n') and U238(n,f) have maxima in the fuel and minima in the graphite, whereas the opposite conditions are true for the remainder of the reactions, which are more sensitive to low energy neutrons.

The gross structure of the flux does not have the same tendency for all reactions. This is probably due to slight differences in the axial positions of the different foils in the two elements used. Since we are primarily interested in the fine structure, however, the macroscopic variations are ignored.

The results given in the figures have been used to calculate the following ratio for the non-threshold reaction in the two locations:

X = Mean reaction rate in graphite region
Mean reaction rate in fuel region

These ratios are listed in Table 4. The computations were based on all measured points except those located nearest to the steel walls of the elements; in the latter positions there is an additional local effect on the fine structure due to absorption and scattering in the steel. The mean values of the reaction rate in each region was obtained by assuming a parabolic flux shape within the region.

The number of measured points for the threshold reactions - Inll5(n,n' $\gamma$ ) and U238(n,f) - was too small to permit the computation of mean reaction ratios. Amplitude ratios were therefore also calculated for all reactions. These are defined as:

The ratios so obtained are shown in Table 5.

The limits of error given in Tables 4 and 5 refer to standard deviations due to counting statistics. The total errors may be somewhat larger in the case of the U238(n,f) reaction because of normalization difficulties due to the non-exponential decay.

Table 4. Ratio of mean reaction rate in graphite to mean reaction rate in fuel, X

Reaction	Core centre	Core-reflector boundary
Mn55(n, γ)	1.052 ± 0.002	1.066 ± 0.002
U238(n,γ)	$1.031 \pm 0.003$	1.058 ± 0.003
Cu63(n,γ)	1.019 ± 0.004	1.035 ± 0.003

Table 5. Ratio of reaction rate at centre of graphite to reaction rate at centre of fuel, Y

Reaction	Core centre	Core-reflector boundary
Mn55(n,γ)	1.080 ± 0.003	1.101 ± 0.003
U238(n, y)	1.046 ± 0.004	1.088 ± 0.004
Cu63(n, y)	1.029 ± 0.005	1.054 ± 0.004
U238(n,f)	$0.938 \pm 0.003$	_
Inl15(n, n')	0.951 ± 0.003	0.950 ± 0.005

The fine structure variations are largest for Mn55. This reaction is more sensitive to low energy neutrons than any of the other reactions [2]. It is the strong absorption of low energy neutrons in the fuel which causes the large variations in this case.

The U238(n, $\gamma$ ) reaction is also depressed considerably in the fuel and here the resonance shielding effect contributes to the result, particularly at the core-reflector boundary. The relative magnitude of the resonance contribution has not been studied quantitatively, however.

The  $Cu63(n,\gamma)$  cross section does not increase so rapidly with decreasing energy as those of the preceding reactions, and the variations in reaction rate are, in consequence, less pronounced.

The threshold reactions,  $Inl15(n, n'\gamma)$  and U238(n, f), which are peaked in the fuel region, give about equal variations although the peaking seems to be slightly less pronounced in the case of In.

In the measurements of the capture reactions in Mn, Cu and U238 the amplitude of the fine structure is larger at the core boundary than at the core centre. This is due to the strong flux depression of low energy neutrons which are relatively more abundant at the core boundary. For the Inl15 threshold reaction, on the other hand, the amplitude appears to be largely equal in the two positions, indicating that the neutron spectrum above 1.5 MeV has the same shape at the core centre and at the core boundary.

No theoretical calculations of the measured fine structure effects have yet been made.

### 5. CONVERSION RATIO MEASUREMENTS

## 5.1 Introduction

The measured quantity was the "modified relative conversion ratio" defined as:

$$RCR = \frac{\left[\frac{U238 \text{ capture}}{U235 \text{ fission}}\right] (FR0 \text{ spectrum})}{\left[\frac{U238 \text{ capture}}{U235 \text{ fission}}\right] (thermal \text{ spectrum})}$$
(1)

From this quantity the true conversion ratio in the fast spectrum, i.e.  $\left[\frac{\text{U238 capture}}{\text{U235 absorption}}\right]$ , can be found using tabulated thermal cross sections and a calculated value of the capture-to-fission ratio of U235.

The capture rate in U238 was detected by counting the Np239  $\gamma$ -activity of irradiated foils using the  $\gamma$ -X-ray coincidence technique and the fission rate in U235 was obtained from the counting rate in a small fission chamber. The experimental method has been described previously [6] and will not be dealt with here, apart from the discussion of a few details peculiar to measurements in a heterogeneous core.

## 5.2 Experimental details

Fig. 14 illustrates how the small U235 fission chamber (diam. 0.6 cm, total length 8 cm, Al-walled) and 0.05 mm thick natural uranium foils were positioned in a fuel element, which was subsequently irradiated at the central position in the FRO reactor. The counting rate in the fission chamber and the activity in the foils irradiated close to its fissile layer were recorded and used to obtain a quantity proportional to the numerator in Eq. (1). The foils distributed along the fuel element were used to obtain an axial scan of the capture rate in U238. A corresponding U235 fission chamber scan was made in a separate measurement with a thin channel inserted into the fuel element.

The heterogeneity of composition in the core region introduces an uncertainty in the results when these are compared with calculations using a homogeneous model. This is in particular true with regard to resonance capture in the thin natural uranium foils. As can be seen in Fig. 14, the foils associated with the fission chamber were both placed close to a fuel plate and should therefore be more shielded than

a foil placed in a homogeneous fuel graphite mixture. The foils used for the axial scan, on the other hand, were positioned between a fuel and a graphite plate. Whether this corresponds to the homogeneous case is doubtful. From fine structure measurements described in the preceding chapter, however, one may infer that the uncertainty due to the heterogeneity is less than  $\pm 1.5$  %, taking the mean reaction rates in the graphite and fuel plates as extreme values.

## 5.3 Results and comparison with theory

The axial distributions of the U238 capture and U235 fission rates are shown in Figs. 15 and 16. The points are normalized to 1 at the core centre and so are the theoretical curves included for comparison. The U238 capture/U235 fission ratio is plotted in Fig. 17 together with a theoretical curve. The scale is chosen to give numbers equal to the conversion ratio in the core (assuming a constant value of  $\alpha$  for U235 of 0.17).

Many other detectors have been used for measurements similar to these, and the results obtained have been described in detail in [2]. The reaction rate distributions included here, however, give much the same kind of information as do other detectors.

The theoretical curves were obtained from two-dimensional 6 group S₄ calculations (TDC) using cross section set 2B developed by Häggblom [2, 5]. The fluxes obtained were multiplied by 6 group U238 (n,γ) and U235 (n,f) cross sections listed in Tables 6 and 7 to give the appropriate reaction rates. The group cross sections were obtained from a condensation routine in the NESPCO programme [7], in which fine structure spectra for the core and reflector regions were first calculated. Thus separate cross section sets are used for the core and copper reflector. This accounts for the discontinuity in the calculated reaction rates at the core-reflector boundary (Figs. 15, 16 and 17).

Table 6. U238 6 group capture cross sections for Assembly 3

1 1	Group Lower One energy No. limit, MeV	U238(n,γ) cross section, b		
-		Core, $\sigma_{\mathbf{x}} = 10b$	Refl., $\sigma_{\mathbf{x}} = \infty$	
1	1.35	0.041	0.046	
2	0.5	0.136	0.136	
3	0.18	0.145	0.144	
4	0.067	0.250	0.247	
5	0.0091	0.434	0.458	
6	0.00012	0.750	2.059	

Table 7. U235 6 group fission cross sections for Assembly 3

Group No.	U235(n,f) cross section, b			
140.	Core, set 2	Core, set 2B	Refl., set 2B	
1	1.33	1.26	1.26	
2	1.21	1.18	1.18	
3	1.36	1.30	1.29	
4	1.69	1.58	1.57	
5	2.35	2.27	2.26	
6	5.06	4.26	6.17	

U235 fission cross sections in 6 groups were computed using primary data according to sets 2 and 2B respectively. While these give significantly different fission rates on an absolute scale, the axial fission distribution, when normalized to 1 at the core centre, is nearly the same in the two cases. Therefore, only the most recent set, based on set 2B, was used in Figs. 12 and 13. The differences between the sets will be discussed below.

In the case of the U238 capture cross section resonance self shielding effects are important. The ERIC-2 [9] programme was used by Häggblom to obtain shielded cross sections, and microscopic data

were available for a number of values of  $\sigma_{\rm x}$ , a quantity sometimes referred to as the "scattering cross section per absorbing atom". It is defined here as

$$\sigma_{\mathbf{x}} = \frac{\sum_{i=1}^{N_{i}} \sigma_{i}}{N_{28}}$$
 in the core
$$\sigma_{\mathbf{x}} = \frac{1}{N_{3} \sqrt{L}}$$
 in the copper reflector

where  $N_i$   $\sigma_i$  is the <u>total</u> macroscopic cross section of material i in the U238 resonance region,  $N_{28}$  is the U238 atomic density and  $\overline{\iota}$  is the mean chord length in the natural uranium detector foil (i.e. twice its thickness).

The first of these expressions refers to a homogeneous mixture; using it for the core region implies that the core is regarded as a homogeneous mixture of the various materials. A value of  $\sigma_{\mathbf{x}} = 14b$  was obtained. Since resonance effects are slight in the core, the value of  $\sigma_{\mathbf{x}} = 10b$ , for which data were available, could be used with little loss of accuracy.

In the copper reflector the only resonance shielding in the foil is that due to the finite thickness of the foil; in this case the equivalence theorem gives the second expression above for  $\sigma_{\mathbf{x}}$ . For a metal foil 0.05 mm thick one obtains  $\sigma_{\mathbf{x}} = \underline{2100b}$ . Here the "nearest" value available was  $\sigma_{\mathbf{x}} = \infty$ , i.e. no self shielding. Using this value, the cross section in the lowest group will be somewhat overestimated.

A comparison of the experimental and theoretical results in Figs. 15, 16 and 17 bear out the following points:

The reaction rates in the reflector is calculated too low. The effect is more pronounced for the U238 capture reaction, which is more sensitive than U235 fission to low energy neutrons. Similar effects have been found for a large number of detectors [2], and the discrepancies are therefore to be associated with the calculated spectrum rather than with cross section uncertainties. The unpredicted neutrons have low energies (< 10 keV) and the calculated spectrum in the reflector is too hard.

- The U238 capture/U235 fission ratio is steadily increasing when going outwards in the reflector, which implies that a continous spectrum softening is taking place. This effect is underrated in the calculation. Separate measurements with shielded manganese foils used as backscatter detectors showed that the contribution to the spectrum softening due to room-reflected neutrons is insignificant.
- While discrepancies between experiment and theory still exist, the reaction rate distributions in the copper reflector are now in substantially better agreement with theory than previously [3]. The improvement is, above all, due to better data for copper in Häggblom's cross section set 2B.

Furthermore, at the core centre the experimental conversion ratio is  $0.406 \pm 0.010$  (estimated max. error). The values using the U235 fission cross sections from sets 2 and 2B (Table 7) are:

Set 2: 0.411 Set 2B: 0.439.

(14 group calculations changed the set 2B value to 0.438.) These figures differ from the experimental one by 1.2% and 8.1% respectively. While the set 2 cross sections are based on BNL-325 (1958 and 1960) data, set 2B includes new Aldermaston data [8]. On the present evidence as well as that provided by other experimental reaction ratios measured at FRO [2], the Aldermaston cross sections are too low. But unfortunately there are so many sources of uncertainty in the calculations that no definite conclusion with regard to any particular cross section can be drawn.

## ACKNOW LEDGEMENTS

The authors are indebted to Dr. H Häggblom for giving much support in the theoretical field. The cooperation of the FRO Operations Group is also gratefully acknowledged.

#### REFERENCES

- 1. LONDEN S-O, Central reactivity measurements on assemblies 1 and 3 of the fast reactor FRO. 1966. (AE-212)
- 2. ANDERSSON T L,
  Reaction rate distributions and ratios in FRO assemblies 1, 2 and 3. 1966.
  (AE-229).
- 3. ANDERSSON T L et al., Experimental studies on assemblies 1 and 2 of the fast reactor FRO. Part 1. 1965. (AE-195).
- 4. HELLSTRAND E et al.,
  Experimental studies on assemblies 1 and 2 of the fast reactor
  FRO. Part 2. 1965.
  (AE-207).
- 5. HAGGBLOM H,
  Theoretical work for the fast zero-power reactor FRO. 1965.
  (AE-194).
- 6. TIREN L I and LUPANDER J-C,
  Measurements of conversion ratio in the fast experimental
  reactor FRO. 1965.
  AB Atomenergi, Sweden (Internal report FFX-10).
- 7. NYMAN K and HÄGGBLOM H,
  Nespco, a programme for calculation of neutron spectrum and
  group crossections in a finite homogeneous medium. 1966.
  AB Atomenergi, Sweden (Internal report RFR-540, RFN-239).
- 8. WHITE P H,
  Measurements of the U neutron fission cross section in the energy range 0.04 MeV to 14 MeV. 1965.
  (EANDC (UK) 51-"S")
- 9. SUMNER H M, ERIC 2, a Fortran program to calculate resonance integrals and from them effective capture and fission cross sections. 1964. (AEEW-R323).

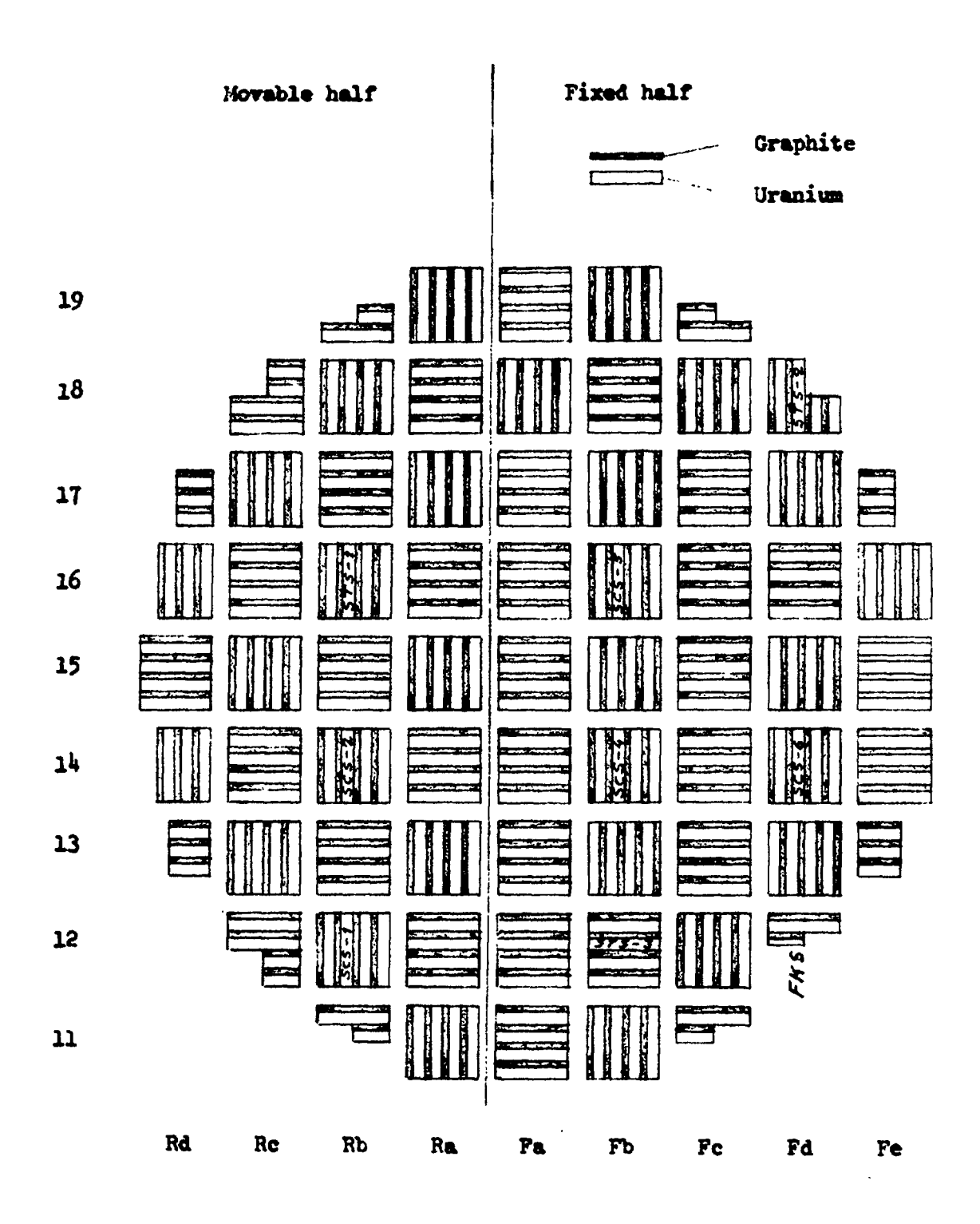


Fig. 1 Normal loading pattern

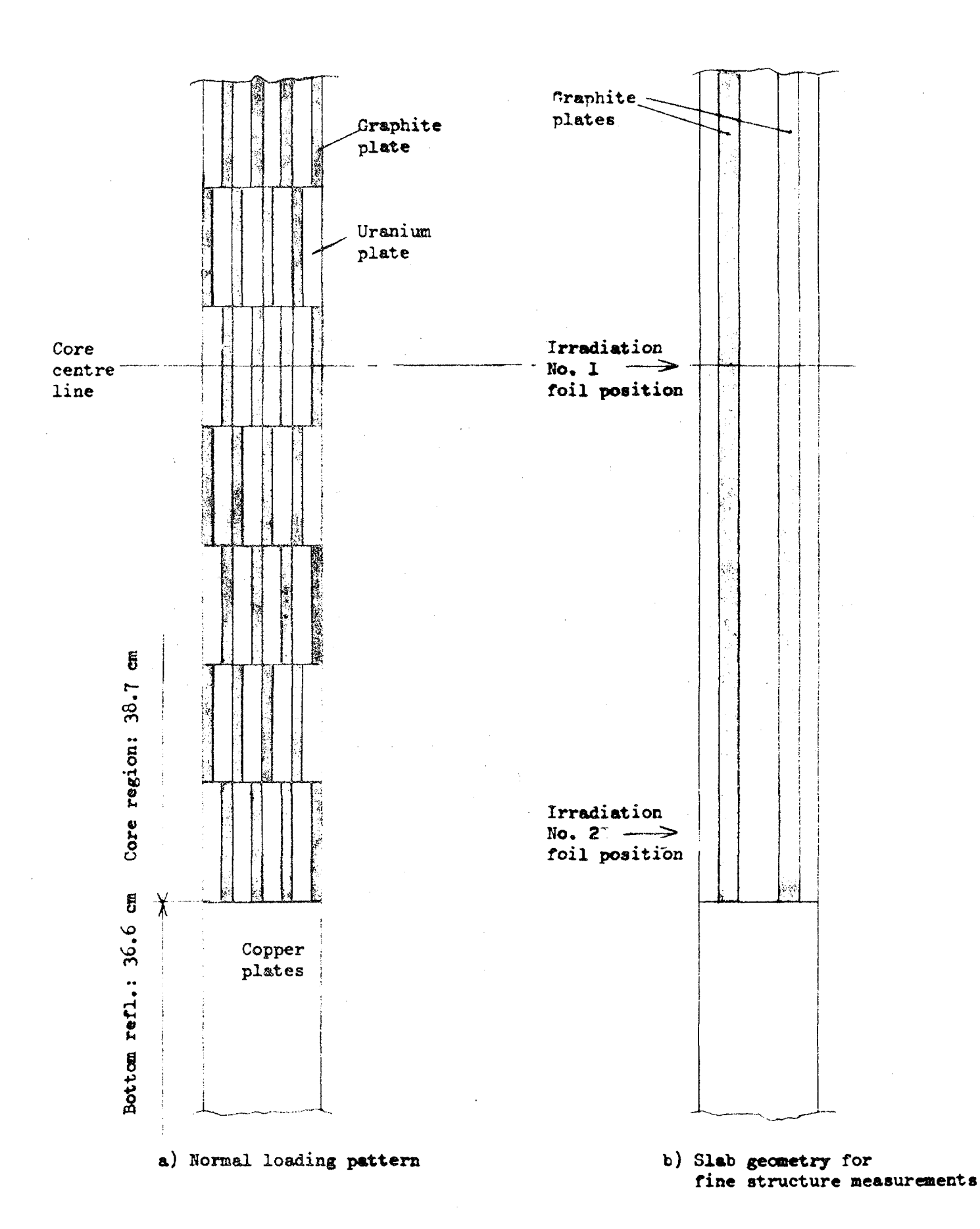


Fig. 2 Loading of fuel elements

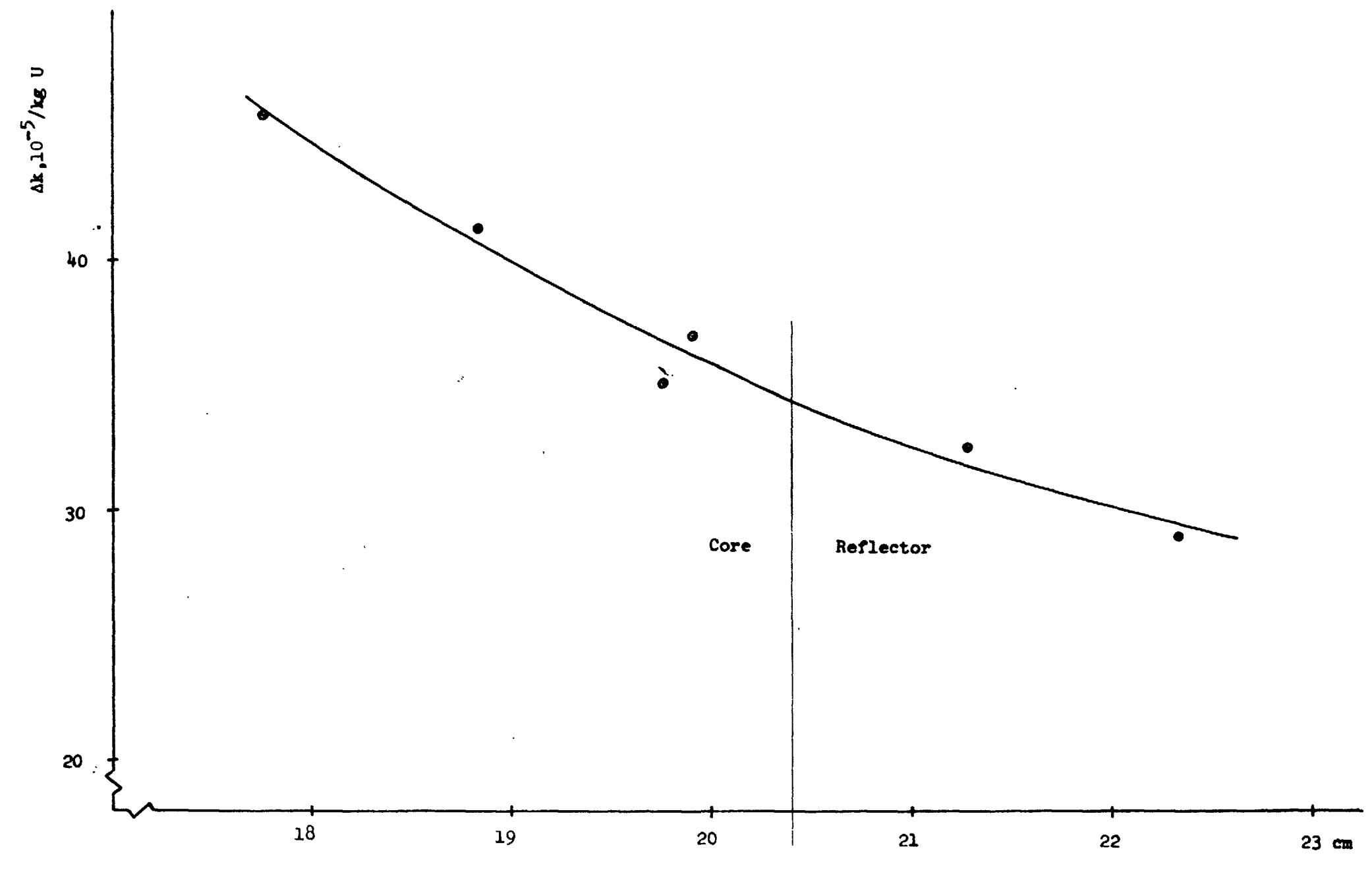


Fig. 3 Fuel-to-copper reactivity difference at core edge

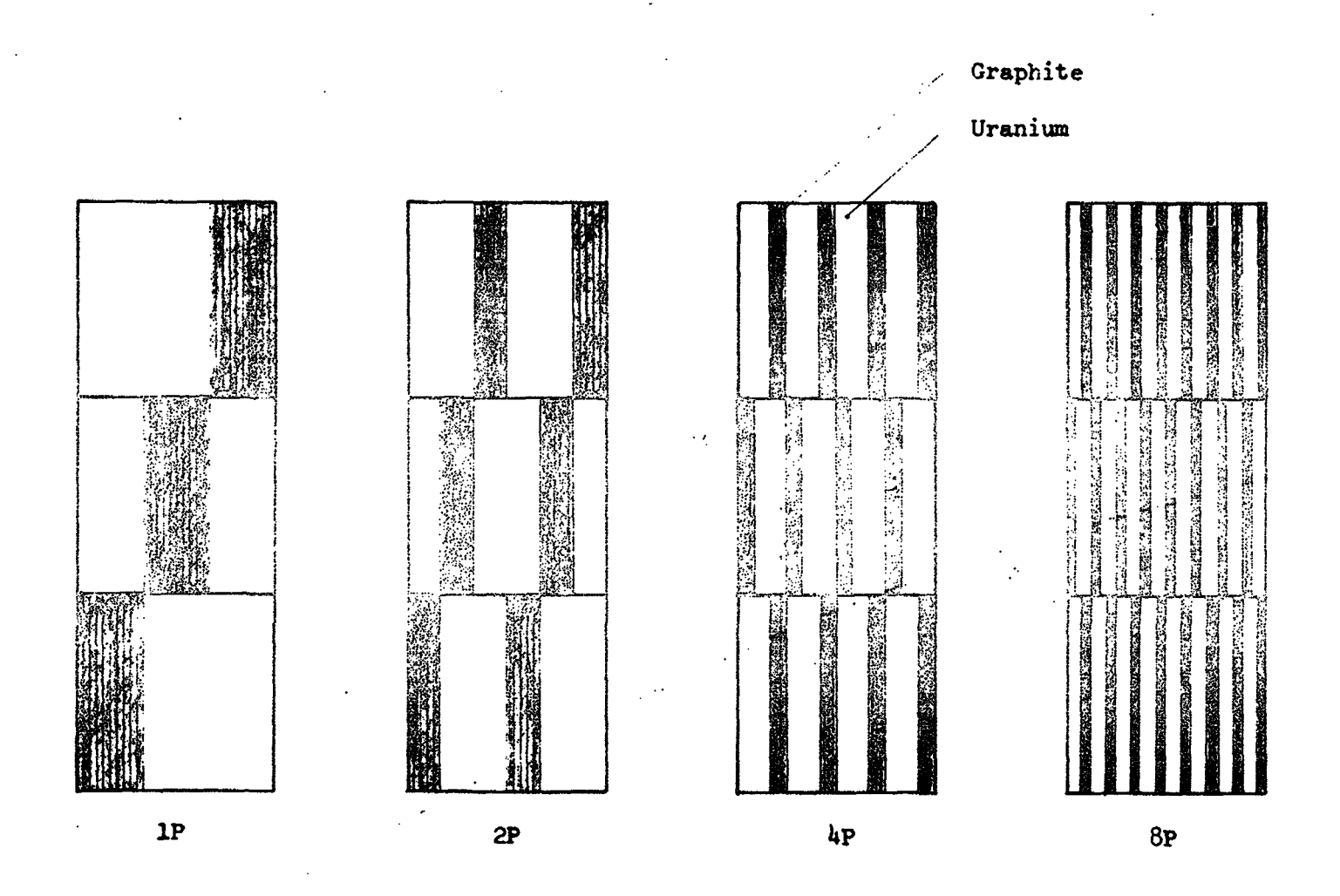


Fig. 4 Bunching of fuel and graphite plates
for heterogeneity experiment

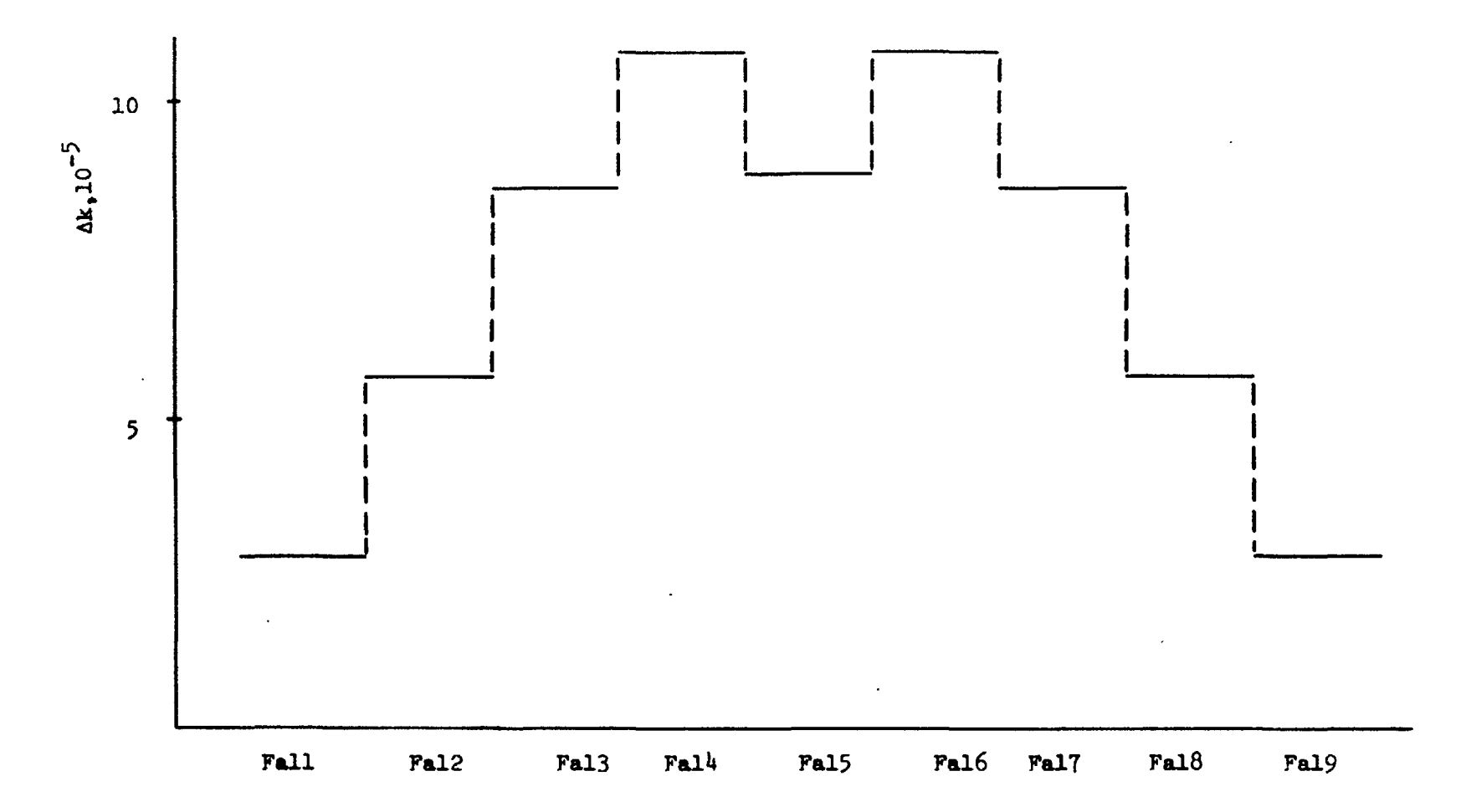


Fig. 5 Reactivity effect of fuel bunching as a function of fuel element position

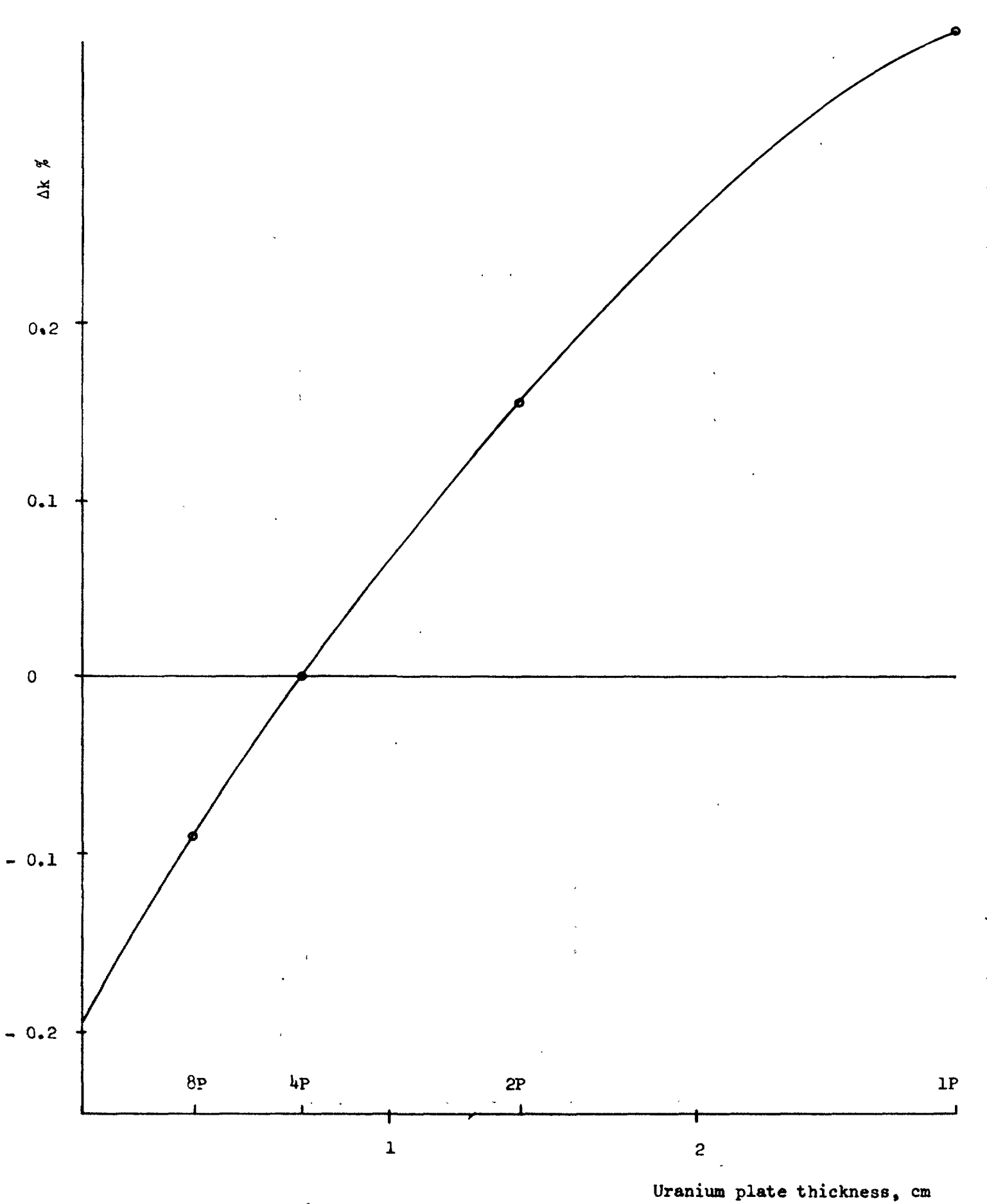


Fig. 6 Reactivity effect of heterogeneity

SCS = Safety rod

STS = Start rod

FKS = Fine control rod

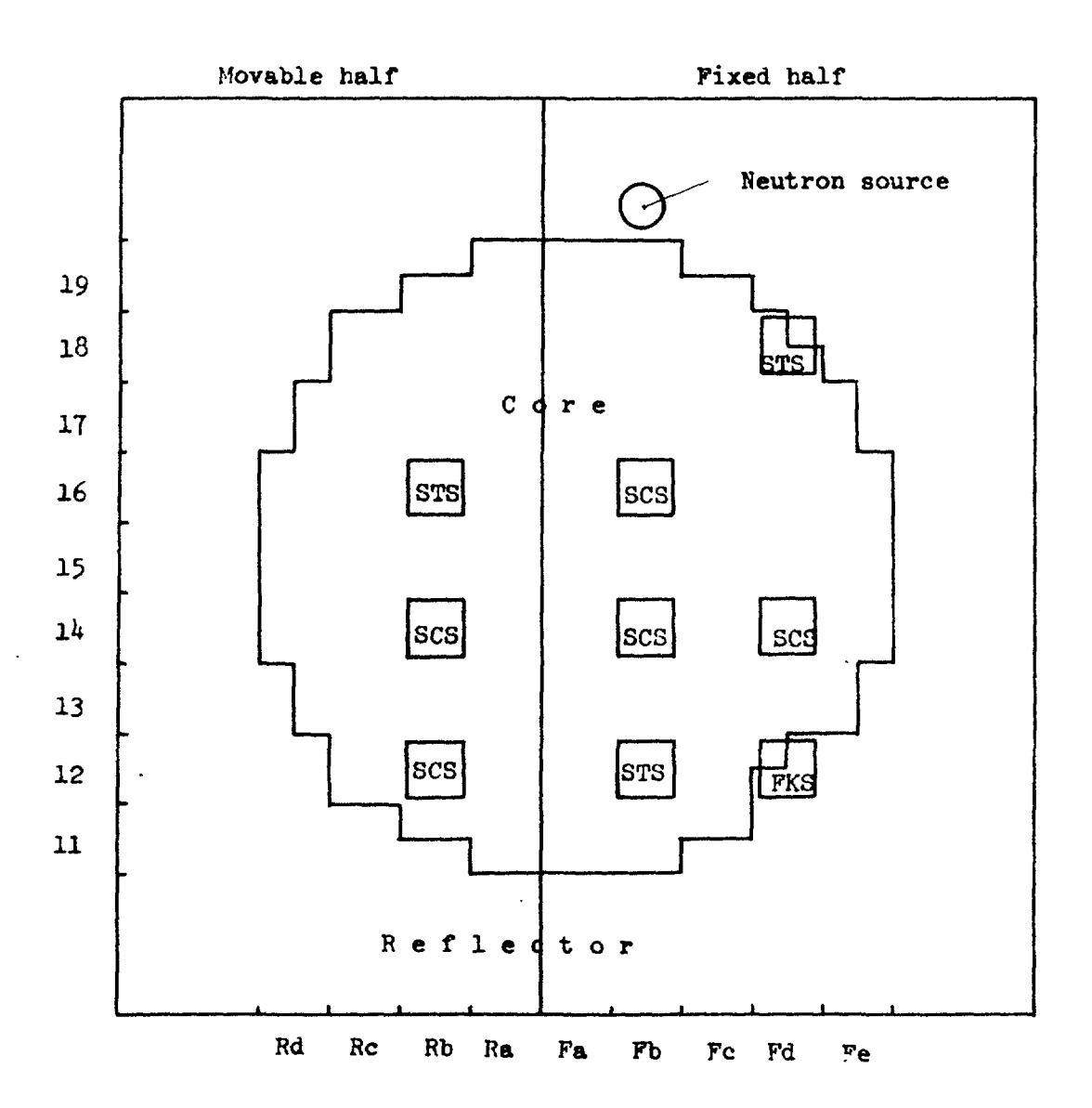


Fig. 7 Control rod positions

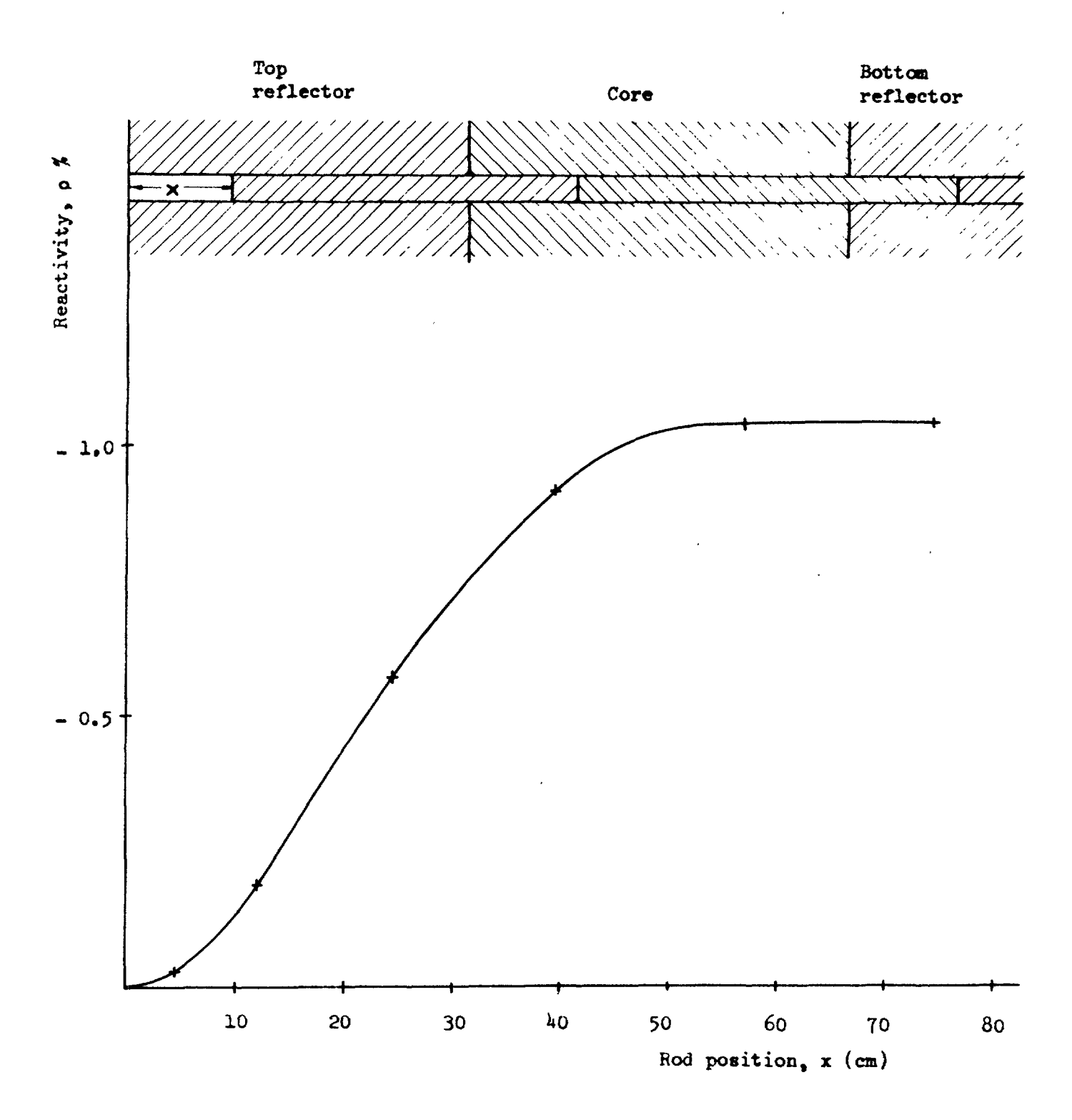


Fig. 8 Reactivity worth as a function of position of start rod 1 (STS1)

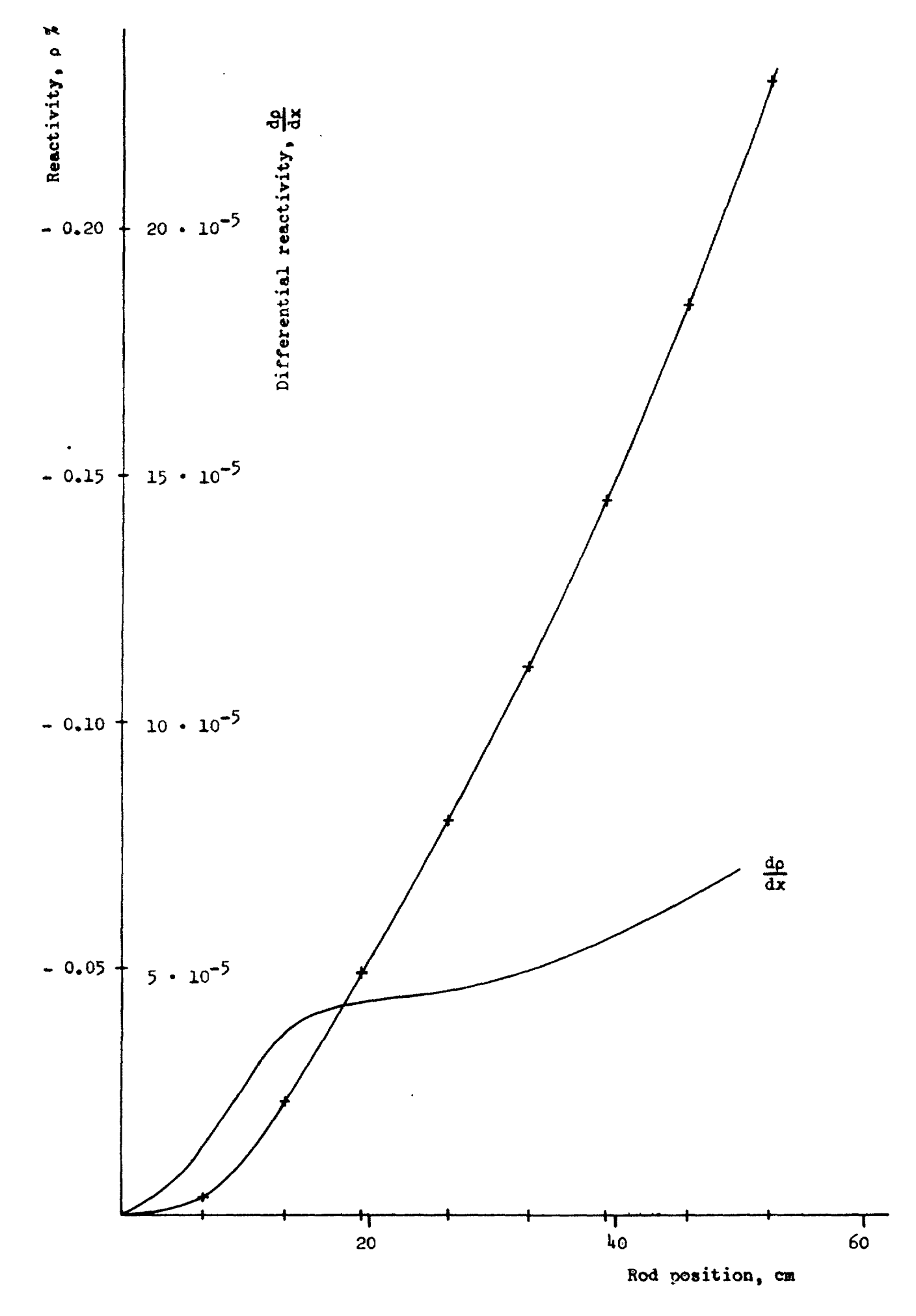


Fig. 9 Reactivity worth as a function of position of the fine control rod (FKS)

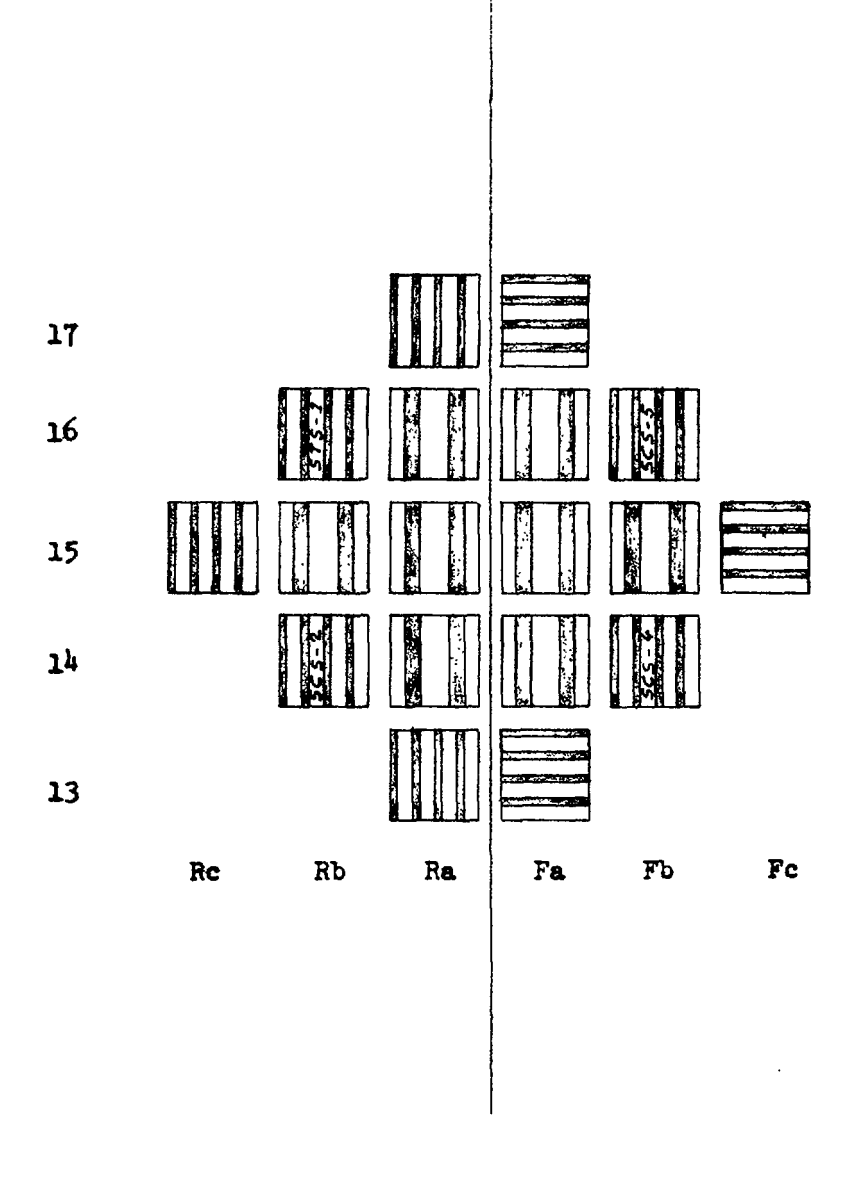


Fig. 10. Loading pattern in central core region for fine structure measurements

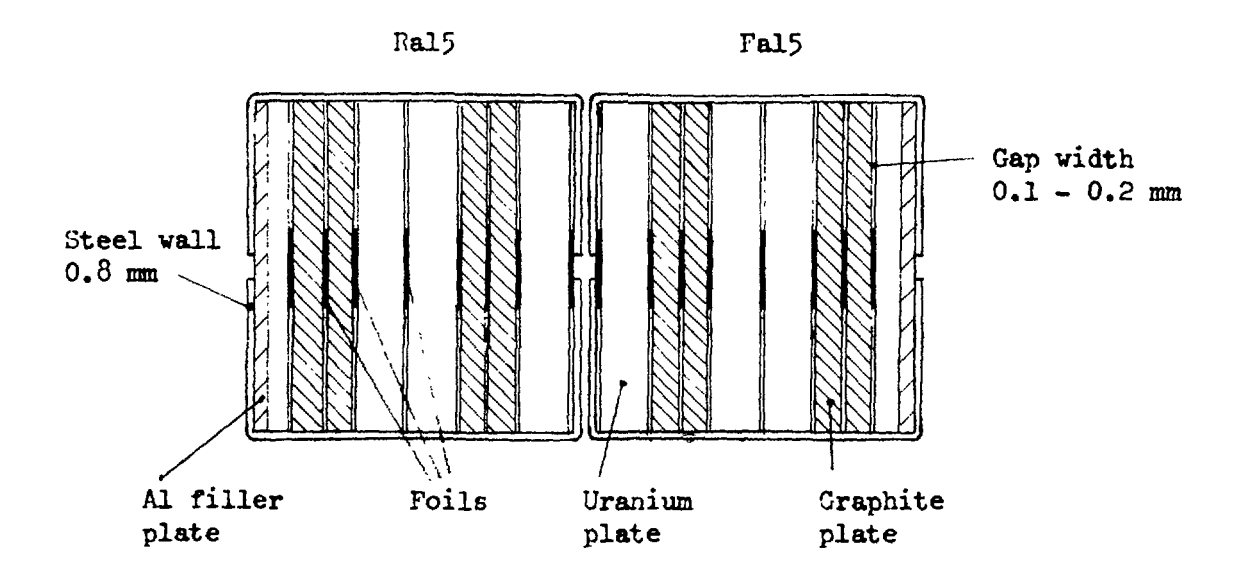


Fig. 11a. Positions for thin foils

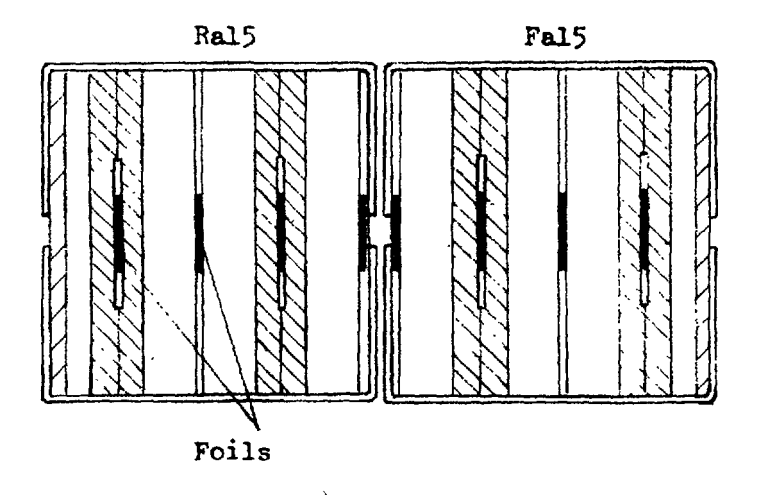


Fig. 11b. Positions for thick foils

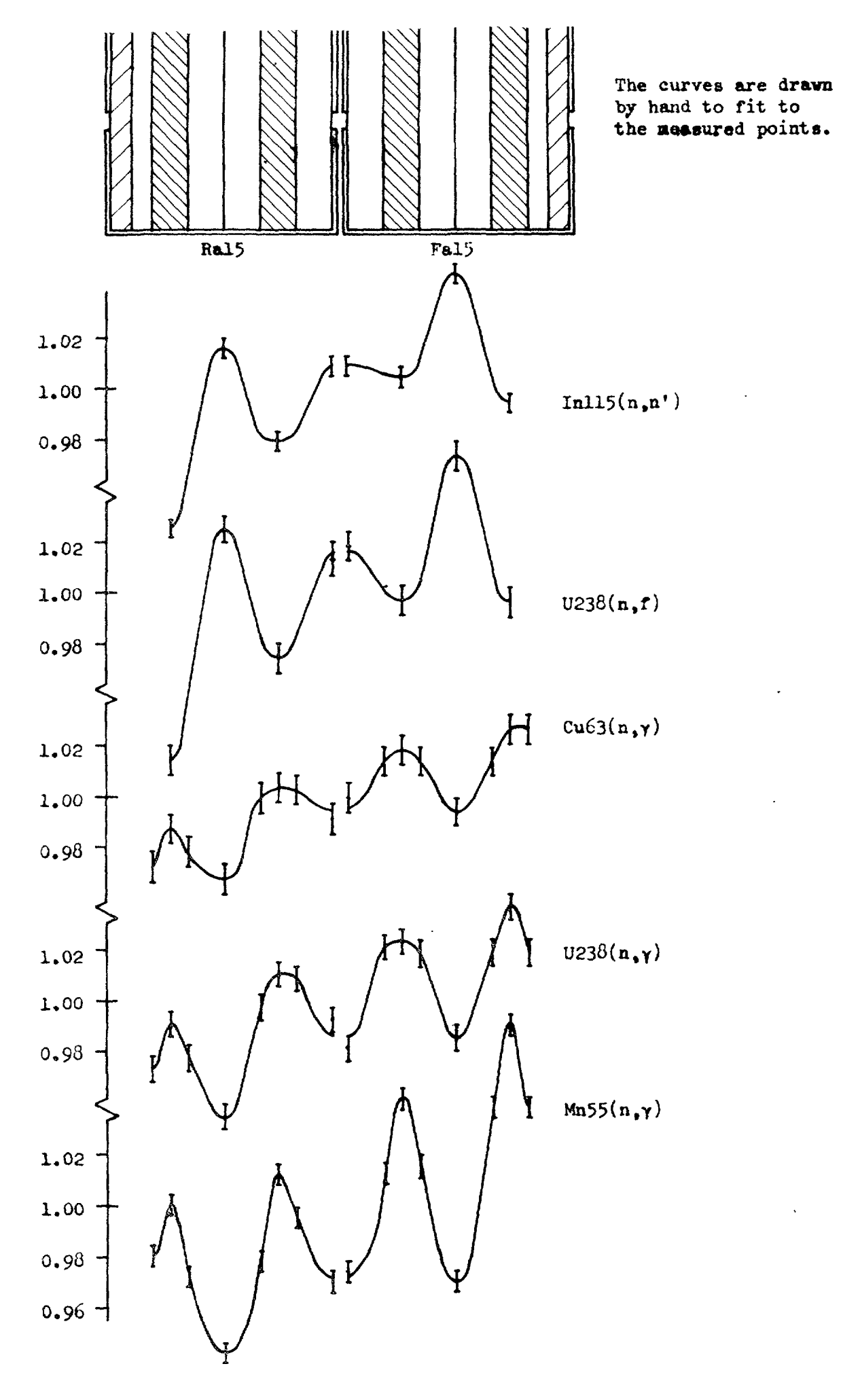


Fig. 12 Reaction rate distributions, core centre

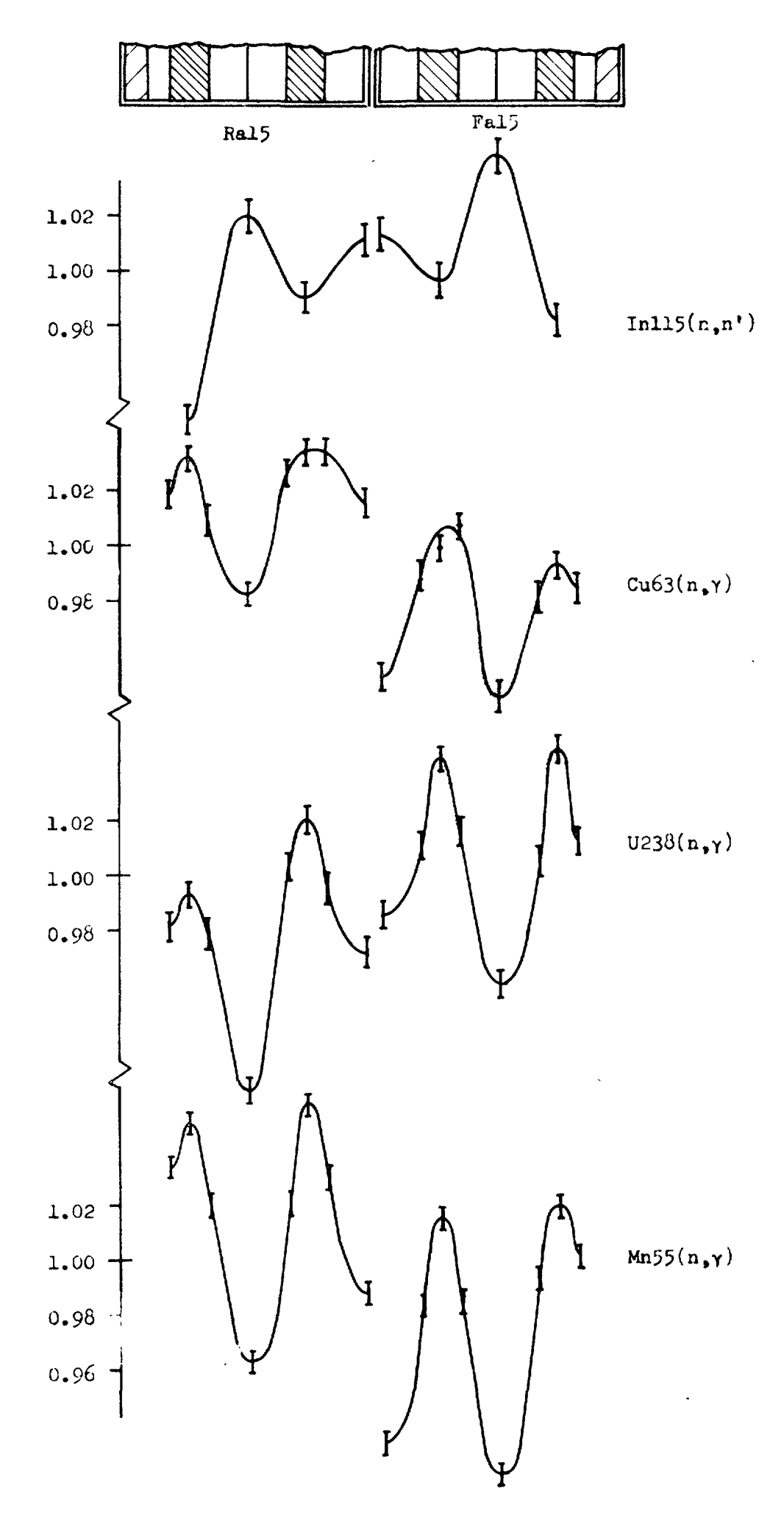


Fig. 13 Reaction rate distributions, core-reflector boundary

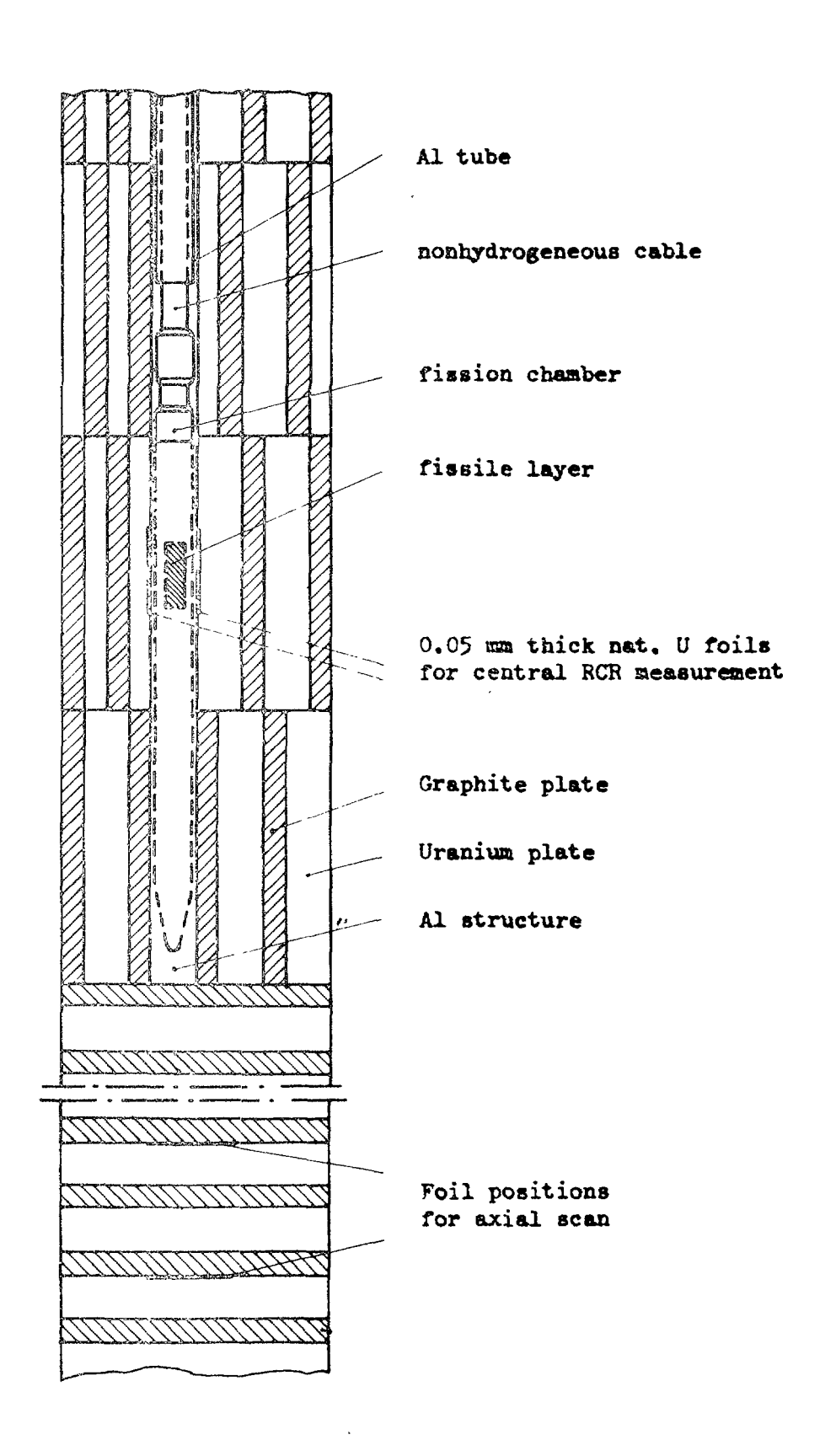


Fig. 14 Irradiation arrangement for conversion ratio measurement

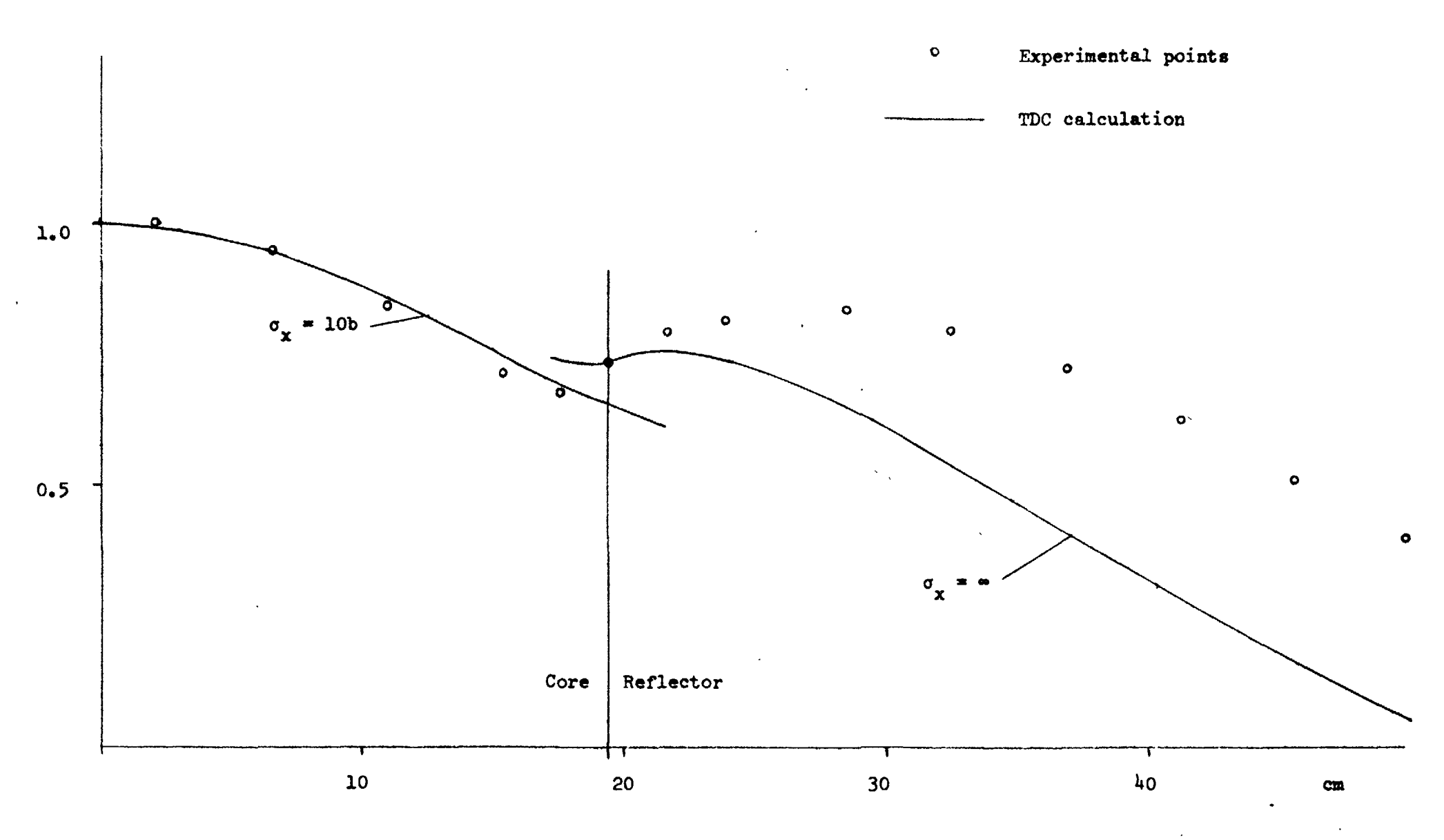


Fig. 15 U238 capture rate, axial distribution

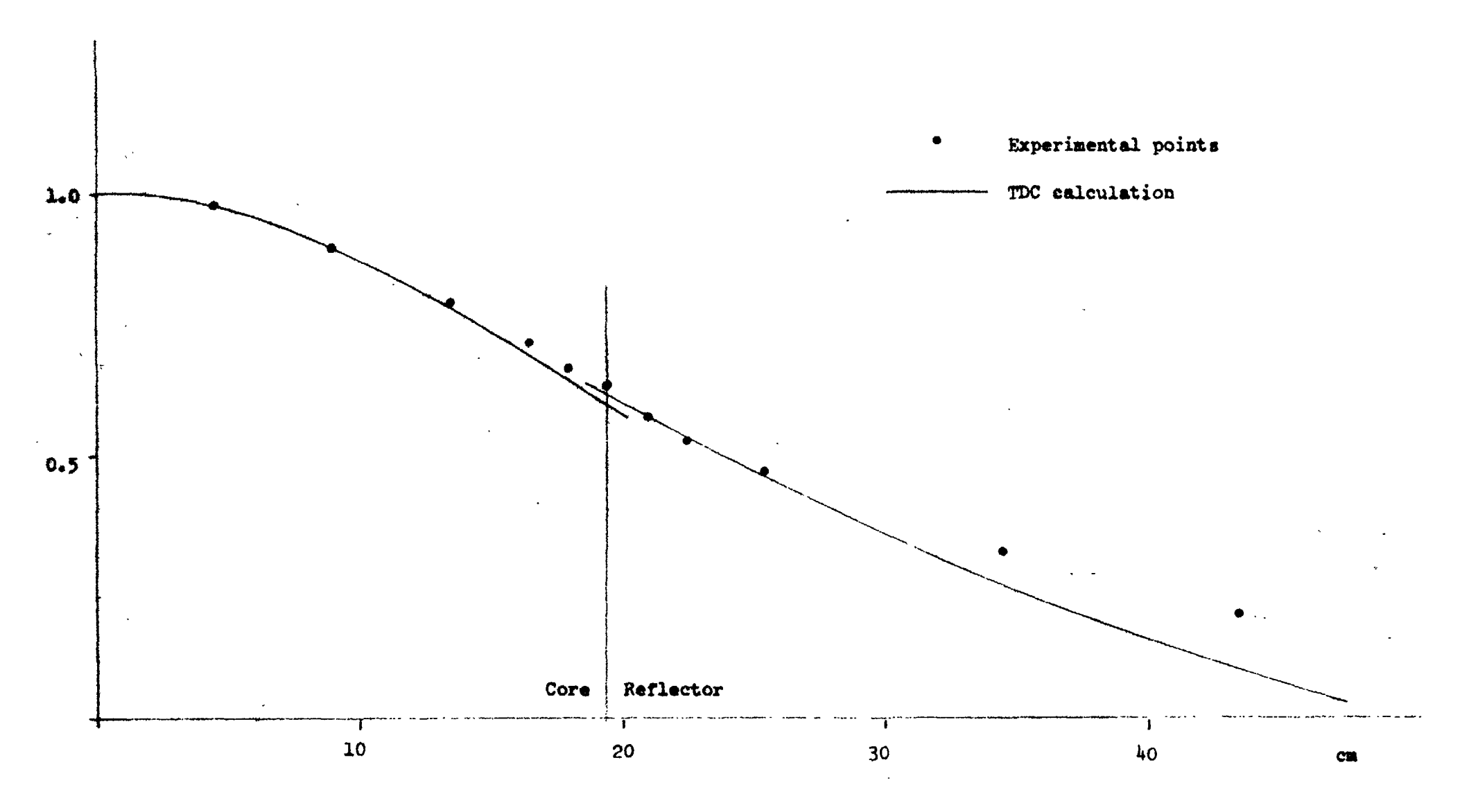


Fig. 16 U235 fission rate, axial distribution

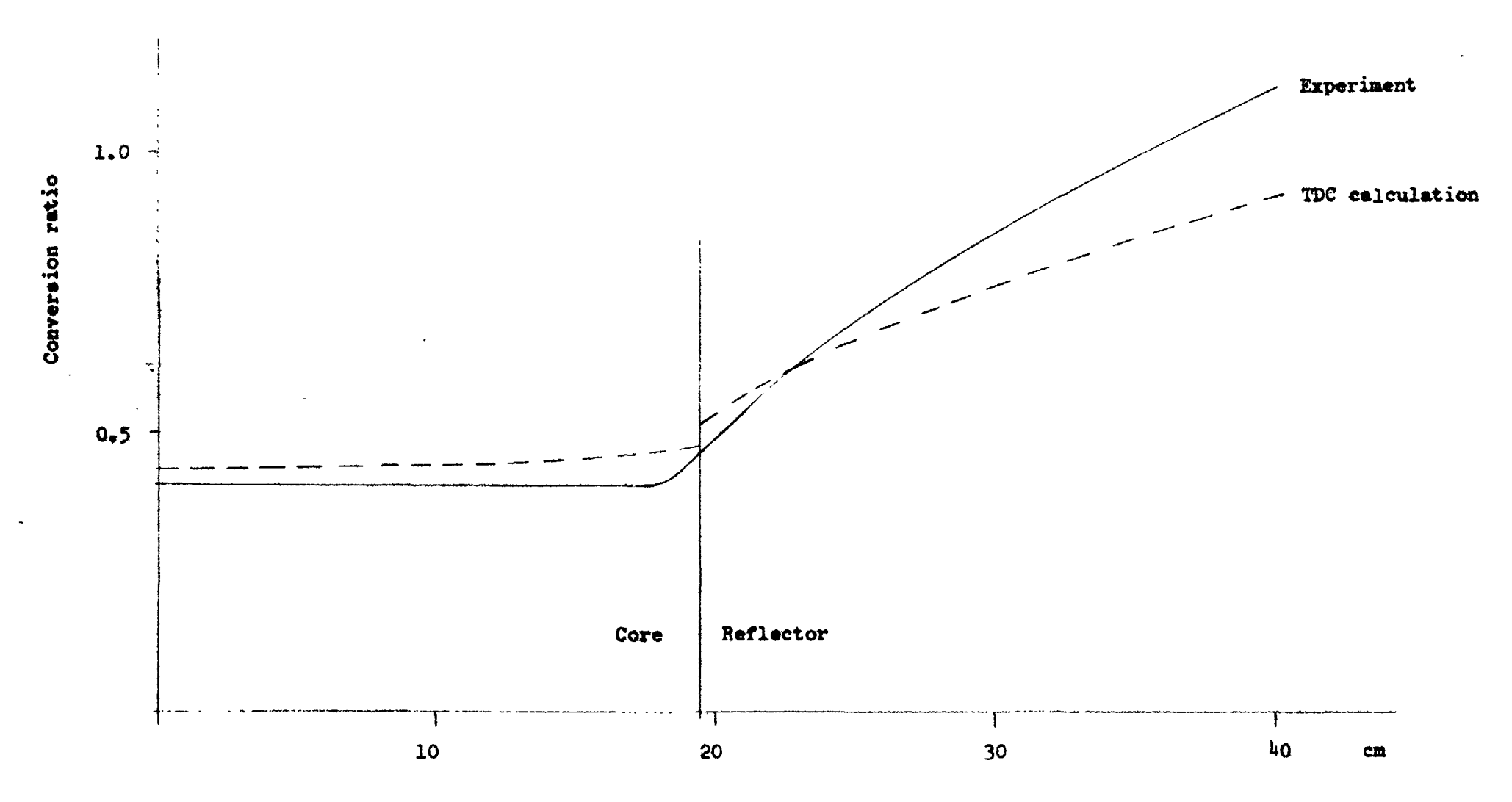


Fig. 17 Axial distribution of conversion ratio

#### LIST OF PUBLISHED AE-REPORTS

- 1-157. (See the back cover earlier reports.)
- 158. A study of the angular distributions of neutrons from the Be⁹ (p,n) B⁹ reaction at low proton energies. By. B. Antolkovic', B. Holmqvist and T. Wiedling. 1964. 19 p. Sw. cr. 8:—.
- 159. A simple apparatus for fast ion exchange separations. By K. Samsahl. 1964. 15 p. Sw. cr. 8:—.
- 160. Measurements of the Fe⁵⁴ (n, p) Mn⁵⁴ reaction cross section in the neutron energy range 2.3—3.8 MeV. By A. Lauber and S. Malmskog. 1964. 13 p. Sw. cr. 8:—.
- 161. Comparisons of measured and calculated neutron fluxes in laminated iron and heavy water. By. E. Aalto. 1964. 15. p. Sw. cr. 8:—.
  162. A needle-type p-i-n junction semiconductor detector for in-vivo measurement of beta tracer activity. By A. Lauber and B. Rosencrantz. 1964. 12 p.
- 163. Flame spectro photometric determination of strontium in water and biological material. By G. Jönsson. 1964. 12 p. Sw. cr. 8:—.
- 164. The solution of a velocity-dependent slowing-down problem using case's eigenfunction expansion. By A. Claessan. 1964. 16 p. Sw. cr. 8:—.
- 165. Measurements of the effects of spacers on the burnout conditions for flow of boiling water in a vertical annulus and a vertical 7-rod cluster. By K. M. Becker and G. Hernberg. 1964. 15 p. Sw. cr. 8:—.
- 166. The transmission of thermal and fast neutrons in air filled annular ducts through slabs of iron and heavy water. By J. Nilsson and R. Sandlin. 1964. 33 p. Sw. cr. 8:—.
- 167. The radio-thermoluminescense of CaSO₄: Sm and its use in dosimetry. By B. Bjärngard. 1964. 31 p. Sw. cr. 8:—.
  168. A fast radiochemical method for the determination of some essential trace elements in biology and medicine. By K. Samsahl. 1964. 12 p. Sw. cr. 8:—.
- 169. Concentration of 17 elements in subcellular fractions of beef heart tissue determined by neutron activation analysis. By P. O. Wester. 1964. 29 p. Sw. cr. 8:-
- 170. Formation of nitrogen-13, fluarine-17, and fluorine-18 in reactor-irradiated H₂O and D₂O and applications to activation analysis and fast neutron flux monitoring. By L. Hammar and S. Forsén. 1964. 25 p. Sw. cr. 8:—.
- 171. Measurements on background and fall-out radioactivity in samples from the Baltic bay of Tvaren, 1957—1963. By P. O. Agnedal. 1965. 48 p. Sw. cr. 8:-
- 172. Recoil reactions in neutron-activation analysis. By D. Brune. 1965. 24 p.
- 173. A parametric study of a constant-Mach-number MHD generator with nuclear ionization. By J. Braun. 1965. 23 p. Sw. cr. 8:—.
- 174. Improvements in applied gamma-ray spectrometry with germanium semi-conductor detector. By D. Brune, J. Dubois and S. Hellström. 1965. 17 p. Sw. cr. 8:—.
- 175. Analysis of linear MHD power generators. By E. A. Witalis. 1965. 37 p.
- 176. Effect of buoyancy on forced convection heat transfer in vertical channels a literature survey. By A. Bhattacharyya. 1965. 27 p. Sw. cr. 8:—.
  177. Burnout data for flow of boiling water in vertical round ducts, annuli and rod clusters. By K. M. Becker, G. Hernborg, M. Bode and O. Erikson. 1965. 109 p. Sw. cr. 8:—.
- 178. An analytical and experimental study of burnout conditions in vertical round ducts. By K. M. Becker. 1965. 161 p. Sw. cr. 8:—.
  179. Hindered El transitions in Eu¹⁵⁵ and Tb¹⁶¹, By S. G. Malmskog. 1965. 19 p.
- Sw. cr. 8:—.
- 180. Photomultiplier tubes for low level Cerenkov detectors. By O. Strindehag. 1965. 25 p. Sw. cr. 8:—.
  181. Studies of the fission integrals of U235 and Pu239 with cadmium and boron filters. By E. Hellstrand. 1965. 32 p. Sw. cr. 8:—.

- 182. The handling of liquid waste at the research station of Studsvik, Sweden. By S. Lindhe and P. Linder. 1965. 18 p. Sw. cr. 8:—.
- 183. Mechanical and instrumental experiences from the erection, commissioning and operation of a small pilot plant for development work on aqueous reprocessing of nuclear fuels. By K. Jönsson. 1965. 21 p. Sw. cr. 8:—.
- Energy dependent removal cross-sections in fast neutron shielding theory. By H. Grönroos. 1965. 75 p. Sw. cr. 8:—.
- 185. A new method for predicting the penetration and slowing-down of neutrons in reactor shields. By L. Hjärne and M. Leimdörfer. 1965. 21 p. Sw. cr. 8:--.
- 186. An electron microscope study of the thermal neutron induced loss in high temperature tensile ductility of Nb stabilized austenitic steels. By R. B. Roy. 1965. 15 p. Sw. cr. 8:—.
- 187. The non-destructive determination of burn-up means of the Pr-144 2.18 MeV gamma activity. By R. S. Forsyth and W. H. Blackadder. 1965. 22 p. Sw. cr. 8:—.
- 188. Trace elements in human myocardial infarction determined by neutron activation analysis. By P. O. Wester. 1965. 34 p. Sw. cr. 8:—.
- An electromagnet for precession of the polarization of fast-neutrons. By O. Aspelund, J. Björkman and G. Trumpy. 1965. 28 p. Sw. cr. 8:—.
- On the use of importance sampling in particle transport problems. By B. Eriksson. 1965. 27 p. Sw. cr. 8:—.
- 191. Trace elements in the conductive tissue of beef heart determined by neutron activation analysis. By P. O. Wester. 1965. 19 p. Sw. cr. 8:—.
- 192. Radiolysis of aqueous benzene solutions in the presence of inorganic oxides. By H. Christensen. 12 p. 1965. Sw. cr. 8:—.
- 193. Radiolysis of aqueous benzene solutions at higher temperatures. By H. Christensen. 1965. 14 p. Sw. cr. 8:—.
- Theoretical work for the fast zero-power reactor FR-0. By H. Häggblom. 1965. 46 p. Sw. cr. 8:—.
- 195. Experimental studies on assemblies 1 and 2 of the fast reactor FRO. Part 1. By T. L. Andersson, E. Hellstrand, S-O. Londen and L. 1. Tirén. 1965. 45 p. Sw. cr. 8:—.
- Measured and predicted variations in tast neutron spectrum when penetrating laminated Fe-D₂O. By E. Aalto, R. Sandlin and R. Fräki. 1965. 20 p. Sw. cr. 8:—.
   Measured and predicted variations in fast neutron spectrum in massive shields of water and concrete. By E. Aalto, R. Fräki and R. Sandlin. 1965. 27 p. Sw. cr. 8:—.

- 198. Measured and predicted neutron fluxes in, and leakage through, a configuration of perforated Fe plates in  $D_2O$ . By E. Aalto, 1965, 23 p. Sw.
- 199. Mixed convection heat transfer on the outside of a vertical cylinder. By A. Bhattacharyya. 1965. 42 p. Sw. cr. 8:—.
- 200. An experimental study of natural circulation in a loop with parallel flow test sections. By R. P. Mathisen and O. Eklind. 1965. 47 p. Sw. cr. 8:-
- 201. Heat transfer analogies. By A. Bhattacharyya. 1965. 55 p. Sw. cr. 8:—.
- 202. A study of the "384" KeV complex gamma emission from plutonium-239. By R. S. Forsyth and N. Ronqvist. 1965. 14 p. Sw. cr. 8:—.
- A scintillometer assembly for geological survey. By E. Dissing and O. Landström. 1965. 16 p. Sw. cr. 8:—.
- 204. Neutron-activation analysis of natural water applied to hydrogeology. By O. Landström and C. G. Wenner. 1965. 28 p. Sw. cr. 8:—.
- 205. Systematics of absolute gamma ray transition probabilities in deformed odd-A nuclei. By S. G. Malmskog. 1965. 60 p. Sw. cr. 8:—.
- 206. Radiation induced removal of stacking faults in quenched aluminium By U. Bergenlid. 1965. 11 p. Sw. cr. 8:—.
- 207. Experimental studies on assemblies I and 2 of the fast reactor FRO. Part 2. By E. Hellstrand, T. L. Andersson, B. Brunfelter, J. Kockum, S-O. Londen and L. I. Tirén. 1965. 50 p. Sw. cr. 8:—.
  208. Measurement of the neutron slowing-down time distribution at 1.46 eV and its space dependence in water. By E. Möller. 1965. 29. p. Sw. cr. 8:—.
  209. Incompressible steady flow with tensor conductivity leaving a transverse magnetic field. By E. A. Witalis. 1965. 17 p. Sw. cr. 8:—.
  200. Methods for the description of surveys and fields in stongly two.

- 210. Methods for the determination of currents and fields in steady two-dimensional MHD flow with tensor conductivity. By E. A. Witalis. 1965. 13 p. Sw. cr. 8:—.
- 211. Report on the personnel dosimetry at AB Atomenergi during 1964. By K. A. Edvardsson. 1966. 15 p. Sw. cr. 8:—.
- 212. Central reactivity measurements on assemblies 1 and 3 of the fast reactor FRO. By S-O. Londen. 1966. 58 p. Sw. cr. 8:—-.
- 213. Low temperature irradiation applied to neutron activation analysis of mercury in human whole blood. By D. Brune. 1966. 7 p. Sw. cr. 8:—.
- 214. Characteristics of linear MHD generators with one or a few loads. By E. A. Witalis, 1966. 16 p. Sw. cr. 8:—.
- 215. An automated anion-exchange method for the selective sorption of five groups of trace elements in neutron-irradiated biological material. By K. Samsahl. 1966. 14 p. Sw. cr. 8:—.
- 216. Measurement of the time dependence of neutron slowing-down and thermalization in heavy water. By E. Möller. 1966. 34 p. Sw. cr. 8:—.
- 217. Electrodeposition of actinide and lanthanide elements. By N-E. Bärring. 1966. 21 p. Sw. cr. 8:—.
  218. Measurement of the electrical conductivity of He³ plasma induced by neutron irradiation. By J. Braun and K. Nygaard. 1966. 37 p. Sw. cr. 8:—.
- 219. Phytoplankton from Lake Magelungen, Central Sweden 1960—1963. By T. Willén. 1966. 44 p. Sw. cr. 8:—.
- 220. Measured and predicted neutron flux distributions in a material surrounding av cylindrical duct. By J. Nilsson and R. Sandlin. 1966. 37 p. Sw. cr. 8:—.
- 221. Swedish work on brittle-fracture problems in nuclear reactor pressure vessels. By M. Grounes. 1966. 34 p. Sw. cr. 8:—.
  222. Total cross-sections of U, UO₂ and ThO₂ for thermal and subthermal neutrons. By S. F. Beshai. 1966. 14 p. Sw. cr. 8:—.
- 223. Neutron scattering in hydrogenous moderators, studied by the time dependent reaction rate method. By L. G. Larsson, E. Möller and S. N. Purohit. 1966. 26 p. Sw. cr. 8:—.
- 224. Calcium and strontium in Swedish waters and fish, and accumulation of strontium-90. By P-O. Agnedal. 1966. 34 p. Sw. cr. 8:—.
- 225. The radioactive waste management at Studsvik. By R. Hedlund and A. Lindskog. 1966. 14 p. Sw. cr. 8:—.
- 226. Theoretical time dependent thermal neutron spectra and reaction rates in H₂O and D₂O. By S. N. Purohit. 1966. 62 p. Sw. cr. 8:—.
- 227. Integral transport theory in one-dimensional geometries. By I. Carlvik. 1966. 65 p. Sw. cr. 8:—.
- 228. Integral parameters of the generalized frequency spectra of moderators. By S. N. Purchit. 1966. 27 p. Sw. cr. 8:—.
  229. Reaction rate distributions and ratios in FRO assemblies 1, 2 and 3. By T. L. Andersson. 1966. 50 p. Sw. cr. 8:—.
- 230. Different activation techniques for the study of epithermal spectra, applied to heavy water lattices of varying fuel-to-moderator ratio. By E. K. Sokolowski. 1966. 34 p. Sw. cr. 8:—.
- 231. Calibration of the failed-fuel-element detection systems in the Agesta reactor. By O. Strindehag. 1966. 52 p. Sw. cr. 8:—.
- 232. Progress report 1965. Nuclear chemistry. Ed. by G. Carlesan. 1966. 26 p.
- 233. A Summary Report on Assembly 3 of FRO. By T. L. Andersson, B. Brunfelter, P. F. Cecchi, E. Hellstrand, J. Kockum, S-O. London and L. I. Tirén. 1966. 34 p. Sw. cr. 8:—.

#### Förteckning över publicerade AES-rapporter

- 1. Analys medelst gamma-spektrometri. Av D. Brune. 1961. 10 s. Kr 6:-.
- Besträlningsföröndringar och neutronatmosfär i reaktortrycktankar några synpunkter. Av M. Grounes. 1962. 33 s. Kr 6:—.
- Studium av sträckgränsen i mjukt stål. Av G. Östberg och R. Attermo. 1963. 17 s. Kr 6:—.
- Teknisk upphandling inom reaktorområdet. Av Erik Jonson. 1963. 64 s. Kr 8:—.
- Agesta Kraftvärmeverk. Sammanställning av tekniska data, beskrivningar m. m. för reaktordelen. Av B. Lilliehöök. 1964. 336 s. Kr 15:—. Atomdagen 1965. Sammanställning av föredrag och diskussioner. Av S. Sandström. 1966. 321 s. Kr 15:—.

Additional copies available at the library of AB Atomenergi, Studsvik, Nyköping, Sweden. Transparent microcards of the reports are obtainable through the International Documentation Center, Tumba, Sweden.